JOURNAL OF MATERIALS PROCESSING TECHNOLOGY 198 (2008) 454–462



journal homepage: www.elsevier.com/locate/jmatprotec

Research on molten pool temperature in the process of laser rapid forming

Tan Hua, Chen Jing, Lin Xin, Zhang Fengying, Huang Weidong*

State Key Laboratory of Solidification Processing, Northwestern Polytechnical University, Xi'an 710072, China

ARTICLE INFO

Article history:
Received 23 July 2006
Received in revised form 5 June 2007
Accepted 22 June 2007

Keywords:
Laser rapid forming
Molten pool temperature
Laser cladding
Temperature measure
Cladding thickness

ABSTRACT

A temperature measurement system has been developed by using a two-color infrared thermometer. The real-time tracking and fixed-point measurement were achieved during the LRF process. The influences of laser processing parameters on the temperature of molten pool was investigated, such as powder feed rate, scanning velocity of laser beam, laser power, spot diameter, shielding gas flow rate and powder feeding position. The control scheme of the single layer thickness was discussed and the relationship between the molten pool temperature and the cladding thickness was build.

© 2007 Elsevier B.V. All rights reserved.

1. Introduction

In recent years, with the rapid development of rapid prototyping (RP) and laser cladding, a new additive manufacturing technology, laser rapid forming (LRF), has been developed. LRF can build full density metal components directly from a CAD model without using dies. It could potentially improve the processing flexibility and save process period and manufacturing cost to a large extent. After the CAD model of the component was built and sliced electronically into a sequence of layers which defined the regions of the component, a metal component was fabricated directly through laser cladding layer by layer. Many methods with the same basic process of fabricating a component have been developed, but referred to by different names, such as laser engineered net shaping (LENS) (Keicher et al., 1997; Griffith et al., 1999), direct light fabrication (DLF) (Wu and Mei, 2003), Laser-Based Additive Manufacturing (LBAM) (Hu et al., 2002; Hu and Kovacevic, 2003), and so on.

The molten pool temperature is an important controlling parameter during the LRF process which directly dominates metallurgical quality and forming accuracy of the part. In order to fabricate components with appropriate properties, comprehensive understanding of the thermal behavior during the LRF process should be necessary. Through monitoring the molten pool temperature and feeding it back to the controller, the LRF process with closed loop control can be achieved. Thus, the geometric properties (shape accuracy, surface finish) as well as the material mechanical properties (strength, ductility) of a component can be well coupled with the process design of the part.

To date, thermal behavior of the molten pool has been investigated by some researchers through the thermal signal monitoring and process modeling. Griffith et al. (Griffith et al., 1999) used thermocouple and imaging techniques to monitor the thermal signature during the LRF process, and study the solidification behavior, residual stress, and microstructural evolution which were determined by the thermal history. Jendrzejewski et al. (Jendrzejewski et al., 2004) and Han et al. (Han et al., 2004) investigated the thermal behavior of laser cladding by thermal modeling. Hand et al. (Hand and Fox, 2000) have

* *Corresponding author*. Tel.: +86 29 88494001; fax: +86 29 88494001.
E-mail addresses: tannwpu@gmail.com (T. Hua), Huang@nwpu.edu.cn (H. Weidong).
0924-0136/$ – see front matter © 2007 Elsevier B.V. All rights reserved.
doi:10.1016/j.jmatprotec.2007.06.090

STRATASYS, INC. EXHIBIT 2016
IPR2025-00257, Page 1

Table 1 – The chemical composition of the materials (wt.%)

	Al	B	C	Co	Cr	Fe	Mo	Ni	Si	Ti	W	Zr	Mn	Nb
Rene 88DT powder	2.2	0.02	0.04	14.0	17.0	<0.5	4.0	Bal	<0.2	3.3	4.2	0.04	–	3.5
Ni20	–	1.22	0.03	–	0.2	0.45	–	Bal	0.95	–	–	–	–	–
316L stainless steel	–	–	0.03	–	16.8	Bal.	2.2	13.8	0.75	–	–	–	0.3	–

also carried out temperature measurement and realized the control of the laser power by using pyrometer. However, the influences of the processing parameters on the thermal behavior and the relationship between the molten pool temperature and the cladding geometric sizes have not been investigated systematically. Lin et al. (Lin and Steen, 1998) measured the temperature of the formed layer by an IR pyrometer and estimated the powder efficiency through an inverse calculation of the boundary temperature obtained from observed surface temperature. Although lots of studies on real-time monitoring have been reported, the present understanding of the thermal behavior during LRF still mainly depended on numerical simulation.

In this paper thermal monitoring techniques were described, the influences of the processing parameters on the thermal behavior of the molten pool were also investigated, and the precision control strategy was discussed based on the temperature measurement.

2. Experiment

The LRF experiments were carried out on a LRF system which consists of a 5 kW continuous wave CO_2 laser, a four-axis numerical control work table, a powder feeder and a lateral nozzle. A temperature measurement system was built up by using a two-color infrared thermometer with an absolute accuracy of 10 K, relative accuracy of 5 K, and response time of 10 ms. The measurement system was calibrated by the ultra high temperature blackbody calibrator. The spectrum was collected by reimaging lens and directed to a pyrometer by the fiber optic cable. During two-color measurement, since intensities at two operating wavelengths which have same effect are compared in the pyrometer, changes in target emissivity have little effect on the temperature value obtained. In addition, the thermometer allows credible temperature measurements for the clad when the molten pool is partly obliterated by the feeding powders. So a two-color technique is suitable under a worse environment during the LRF process.

The substrate was 316L stainless steel sheet with dimension of 60 mm × 16 mm × 8 mm, and Rene88DT superalloy and Ni20 hot spraying alloy powders with the size of 44–150 μm were used due to their excellent resistance to oxidation. The compositions of the substrate and the powders were listed in Table 1 and their thermal properties were shown in Table 2. In order to eliminate the moisture of the powder particles and clean the surface of the substrates, the powders were dried in a vacuum oven with 120 °C and the surface of the substrates were burnished by using sand paper before experiment.

In order to investigate the influence of processing parameters on the pool temperature, the single layer and multi-layer clad with length of 60 mm along the scanning direction were built with different processing conditions.

Although the materials emissivity have little effect on the temperature measurement by using a two-color technique, the temperature measurement system has also been calibrated for the Rene88DT and Ni20 alloys with a standard PtRh30–PtRh6 thermocouple to achieve the reliable temperature value.

3. Measurement of temperature

3.1. *Real-time tracking measurement*

The sensor of the temperature measuring system was fixed on the laser head (Fig. 1), and the angle between the laser beam and the sensor detecting direction was set to be as least as possible to reduce the error caused by a small molten pool moving along the Z-axis. As the laser cladding was carried out, the sensor moved with the laser head together and aimed at the molten pool all the time.

Fig. 2 showed the real-time temperature variation of a single Ni20 clad with 30 mm length, and the sampling time was 0.1 s. It can be clearly found that the time intervals of both the initial rise stage and final decline stage of the temperature were about 0.2 s.

3.2. *Fixed-point measurement*

In order to understand the thermal behavior in the molten pool, a fixed-point temperature measurement was designed. In such case, the sensor aimed at the midpoint of the track as shown in Fig. 3. When laser beam scanned via the midpoint of the clad, the changes of the temperature of the midpoint would be recorded by the measurement system. A rise and decline stage of the temperature can also be observed during the measurement, and the decline corresponds to the cooling

Table 2 – The thermal properties of the materials

	Thermal conductivity (W/(m °C))	Heat capacity (J/kg °C)	Solidus temperature (°C)
Rene 88DT powder	17.47	490	1360
Ni20	87.8	443.5	1070
316L stainless steel	21.5	500	1420

STRATASYS, INC. EXHIBIT 2016
IPR2025-00257, Page 2

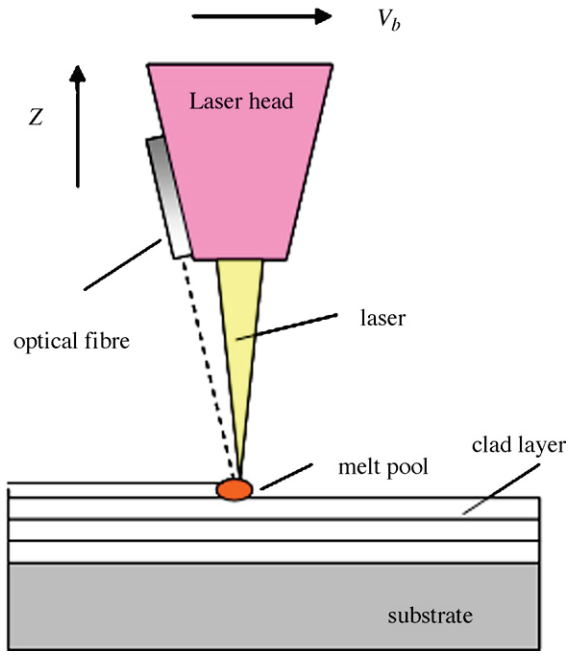


Fig. 1 – Sketch of real-time temperature measurement.

stage. The more abrupt the decline is, the greater the cooling rate is. Fig. 4 shows the in situ temperature record of the midpoint of a single Ni20 clad with the laser power $P = 2100\,W$, spot size $D_b = 2.5\,mm$, and scanning velocity $v_b = 10\,mm/s$. The response time of the thermometer was set to 0.01 s. Based on the assumption that the molten pool is under the steady state in the middle part of the clad with the constant laser scanning velocity, the temperature profile along the scanning direction can be defined as

$$T_1(r^*) = T\left(t_0 + \frac{r^*}{v_b}\right) \quad (1)$$

where $T_1(r^*)$ is the temperature at the distance r^* from the center of molten pool. In this case, the pool center is identical with

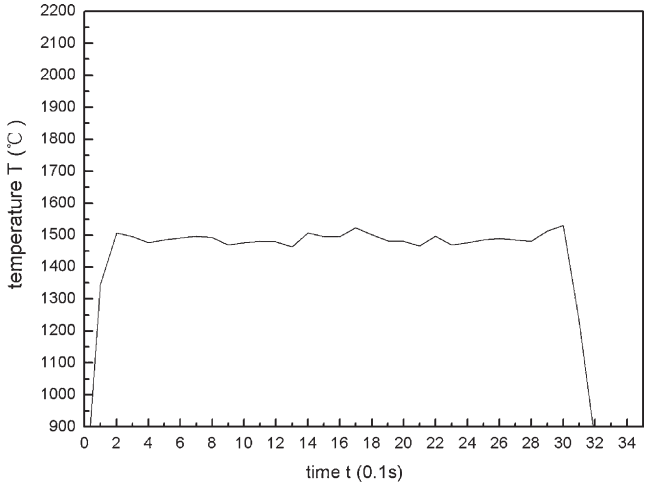


Fig. 2 – Result of real-time temperature measurement in a single cladding.

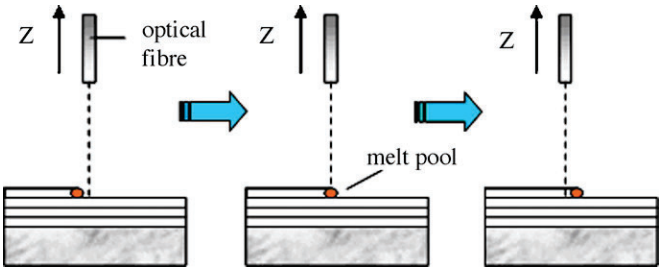


Fig. 3 – Sketch of temperature measurement on specifically position.

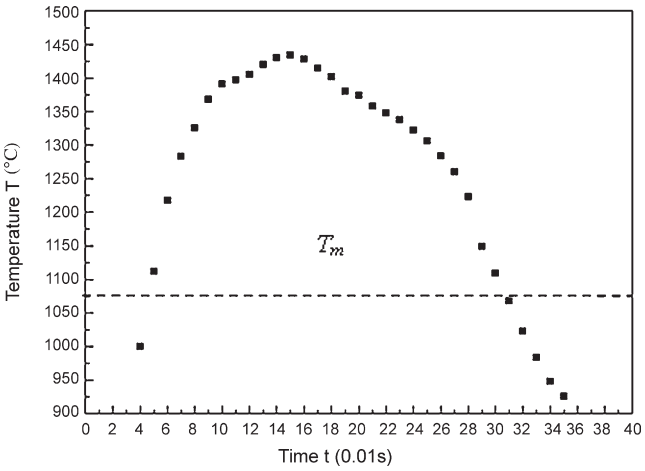


Fig. 4 – Temperature measurement of the specifically position in laser cladding.

the axial of laser beam, v_b is scanning velocity, $T()$ stands for the time dependent temperature and t_0 is the time when laser just pass through the midpoint. The dot line in Fig. 4 illustrates the melting point temperature T_m. The melting length l can be approximately obtained by the product between the scanning velocity and the time when the midpoint is under the melt state, and from the Eq. (1), the temperature decline stage in the midpoint in the Fig. 4 can be transformed into the temperature profile from the center along the scanning direction, as shown in Fig. 5. It can be found that the temperature profiles of the molten pool reveal an interesting non-linearity.

4. Results and discussion

4.1. *The influences of processing parameters on thermal behavior of the molten pool*

4.1.1. *Powder feeding rate*

Fig. 6 shows the influence of the powder feeding rate on the average temperature of the molten pool for a single Ni20 clad. It can be found that the molten pool temperature dropped in the whole course with the increasing of the powder feeding rate. This results from the cooling effect of powder particles. The relatively cool powders play a role of the refrigerant in this case. With the entrance of the more powders to molten pool, the molten pool temperature would decrease.

STRATASYS, INC. EXHIBIT 2016
IPR2025-00257, Page 3

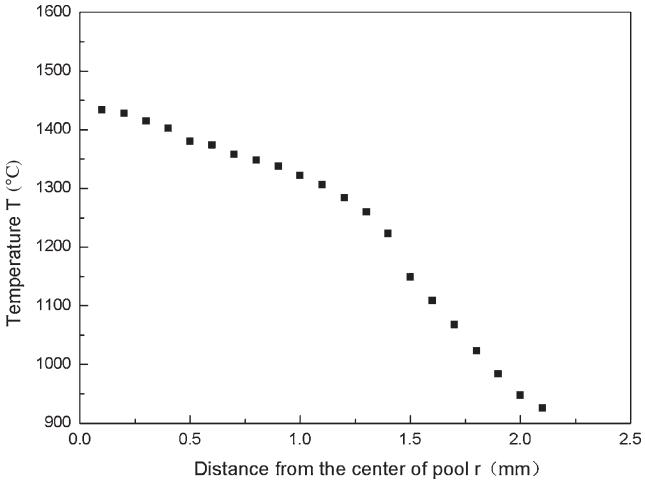


Fig. 5 – Temperature profile of the surface of steady-state melt pool tail.

4.1.2. *Scanning velocity*

Fig. 7 shows the variation of temperature of the molten pool with the scanning velocity by the real time measuring for a single Ni20 clad. From Fig. 7(a), it can be seen that the molten pool temperature varied considerably with the increasing of the scanning velocity. It is due to that there is a decreasing of energy density with the scanning velocity increasing. Fig. 7(b) shows the results obtained by the fixed-point method. It can also be found that temperature profiles have a very similar relationship with the scanning velocity. The scanning velocity for each profile is shown in the legend. It is clear that the length of the molten zone decreases with the increases of the scanning velocity, and the slopes of the tail temperature profiles of the molten pool increases as the scanning velocity decreases.

4.1.3. *Laser power*

Fig. 8(a and b) show the average molten pool temperature and the tail temperature profiles varying with laser power for a single Ni20 clad. It can be found that the average temperature increases with the increasing of the laser power. Not only the heat affected zone was enlarged, but also the cooling rate was increased according to the slope of tail temperature profile with the increasing of the laser power. It is due to that the increase of laser power under the constant spot size caused the increase of the energy density.

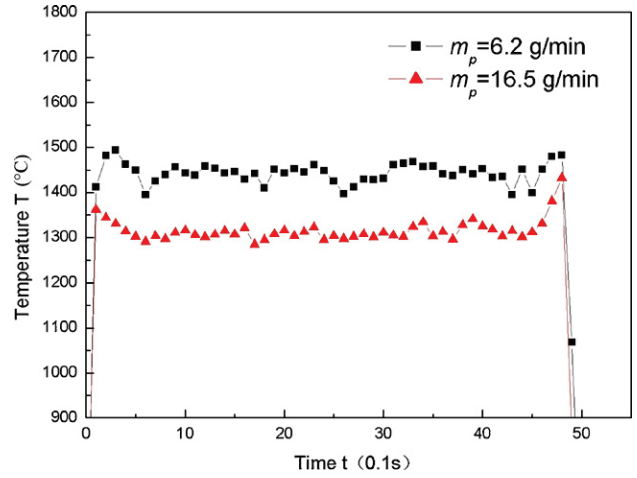


Fig. 6 – Comparison of temperature measurement result with different powder feeding rate.

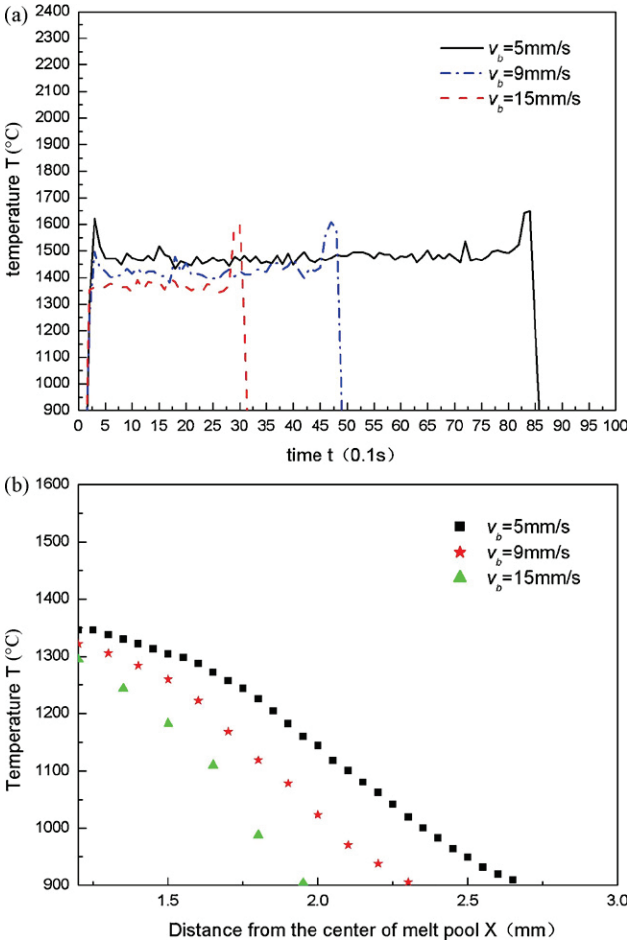


Fig. 7 – Influence of laser scanning velocity on temperature, (a) real-time temperature measurement, (b) fixed-point temperature measurement.

4.1.4. *Laser spot size*

With a fixed laser power, the variation of laser spot size will correspond to the change of the energy density. The laser energy density increases with the decrease of the spot, and a higher temperature gradient can be achieved. The relationship between temperature gradient of molten pool and the spot size during Rene88DT alloy clad can be seen in Fig. 9.

4.1.5. *Shielding gas*

The powder particles were fed into the molten pool with the restriction of shielding gas. In present experiments, the thermal loss caused by shielding gas flow was also investigated. From Fig. 10, it can be found that the average temperature of molten pool declined slightly for a single Ni20 clad till the shielding gas flow flux is up to 20 l/min, it demonstrates that the influence of shielding gas flow flux within the allowed range on the average temperature of the pool field can be neglected.

STRATASYS, INC. EXHIBIT 2016
IPR2025-00257, Page 4

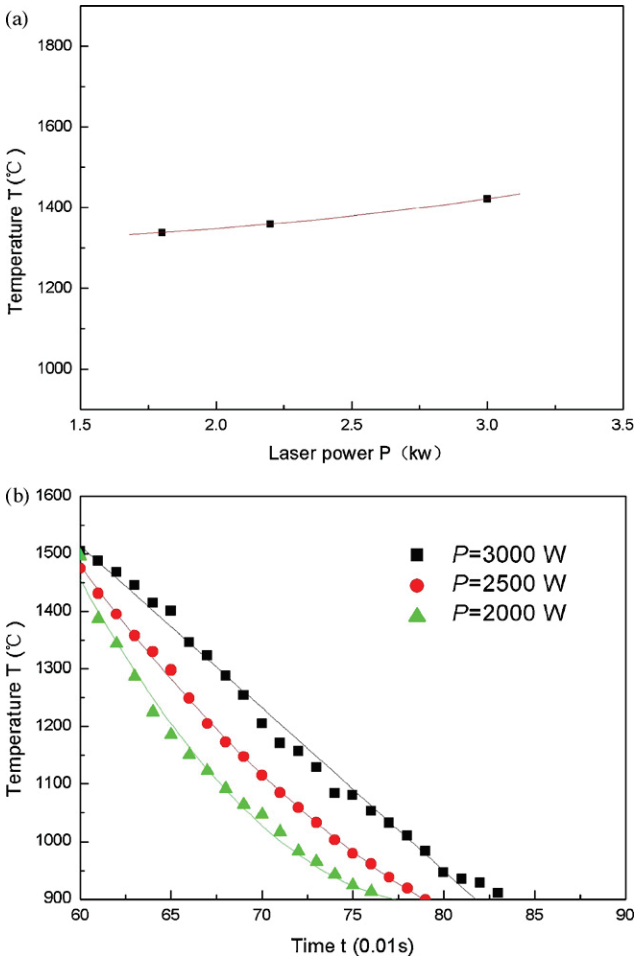


Fig. 8 – Temperature measurement with varying laser power, (a) average temperature during single layer cladding, (b) temperature distribution of the tail of molten pool.

4.2. *Other factors*

Since the powder particles are considered as a kind of refrigerant, the control of drop position of the powder stream on the molten pool is important. That means the relative position between the molten pool and the center of powder stream will have an effect on the molten pool temperature. Fig. 11(a) shows the sketch of the powder feeding position, i.e. the center of the powder stream aims at the head, the center and the tail of the molten pool, respectively. For these three conditions, the shield of the particles injected on the molten pool and the amount of the particles injected into the pool would be dramatically changed. The effects of the relative position on temperature profile of the tail part for a single Ni20 clad were shown in Fig. 11(b). With the position from the head to

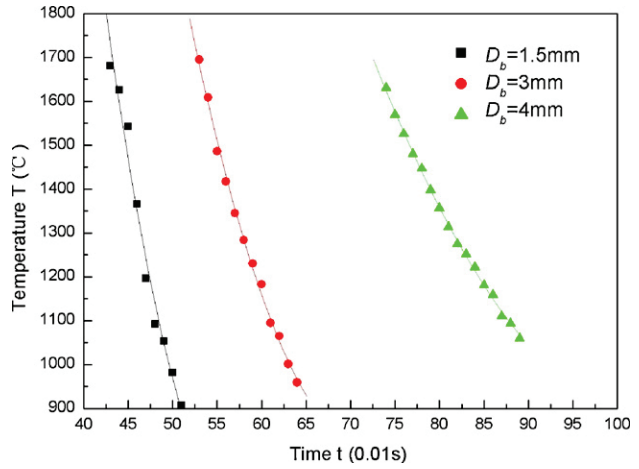


Fig. 9 – Temperature evolvement of melt pool tail with different laser spot diameter.

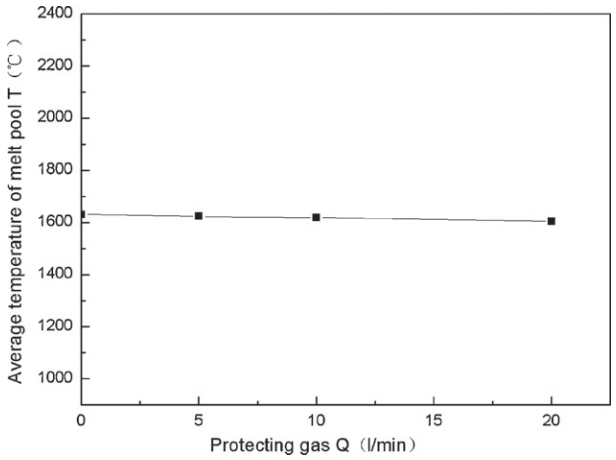


Fig. 10 – Influence of the shield gas on average temperature of melt pool.

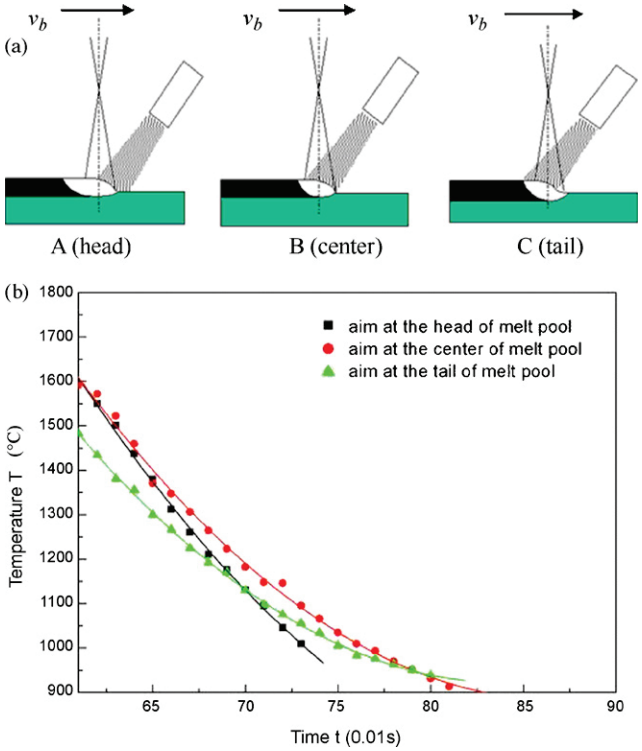


Fig. 11 – Influence of the powder feeding position, (a) sketch of the powder feeding position, (b) cooling curve.

STRATASYS, INC. EXHIBIT 2016
IPR2025-00257, Page 5

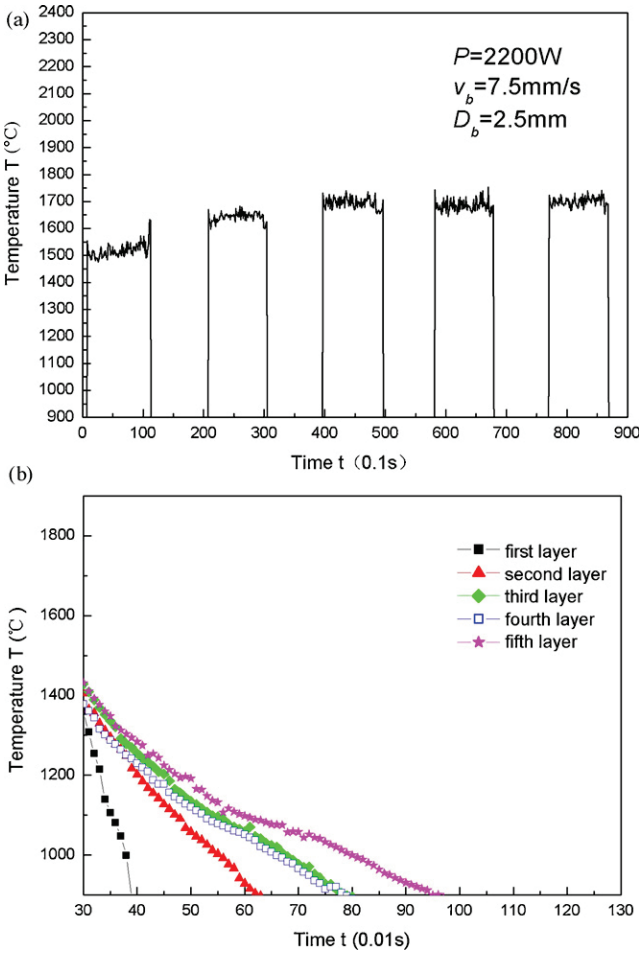


Fig. 12 – Results of the real-time temperature measurement in a multi-layers cladding, (a) real time measurement, (b) cooling curve.

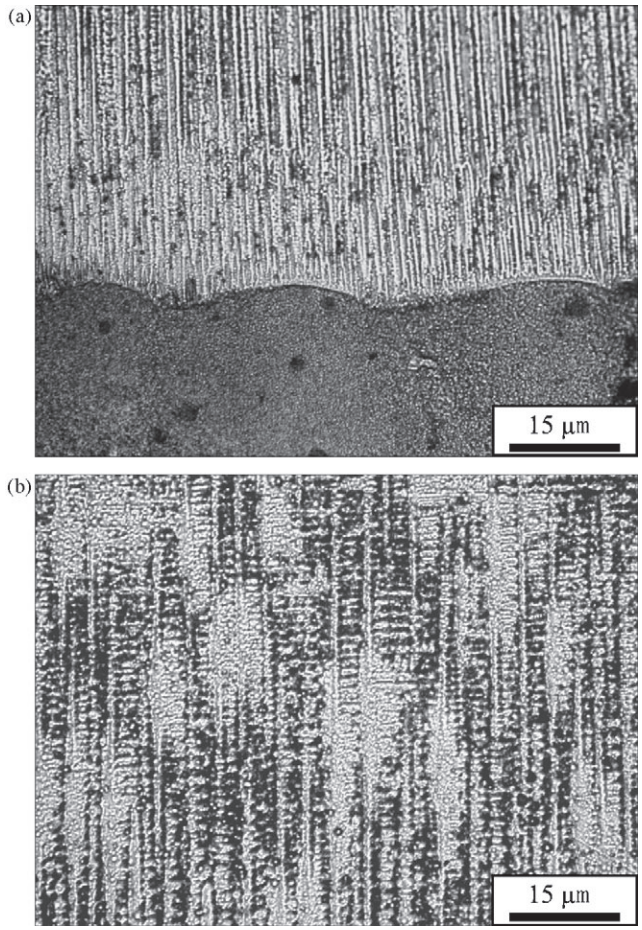


Fig. 13 – Microstructure of Rene88DT alloy sample, (a) Bottom, (b) Top.

the tail, the solid–liquid interface is closer to the center, and the temperature gradient decreases.

Research on the thermal behavior during multi-layer cladding has a great significance to understand the LRF process since multi-layer cladding is a basic way to fabricate the bulk components. Fig. 12(a) shows real time temperature records of the initial five layers during forming a thin Ni20 wall. From Fig. 12, it can be found the molten pool temperature in the first layer is lower than the other four layers, and with the increase of the layer number, the pool temperature gradually rises from about 1500 °C to about 1700 °C. It is due to that, firstly, the original temperature of the substrate was low (room temperature), with the increasing of the layer number, the temperature of the substrate gradually rise. Secondly, with the increasing of the layer number, the thermal conduction mechanism transforms from 3D to 2D, but the input energy keeps constant. With the gradual balance between the input and the output of energy, the temperature will tend to reach steady state. The influence of dilution effect from the substrate to the first pass can be ignored because of a very little dilution. As long as it was ensured that the rise of the reimaging lens was equal to the thickness designed ΔZ, the cooling rate (or the temperature gradient) in each layer could be obtained by the fixed-point measurement. From the curves depicted in the Fig. 12(b), it can be found that the cooling rate (or temperature gradient) first decreases and then inclines to invariableness with the increase of layer number. This is because the temperature of the previous cladding layer was raised with the accumulation of energy, which resulted in the new clad on the hotter substrate. Fig. 13(a and b) show the microstructure of Rene88DT alloy sample at the bottom and the top along the deposition direction, it can be found that the primary dendritic spacing increases with increasing the deposition height and the secondary dendrites grow up gradually. According to the approximate relationship among the temperature gradient, solidification velocity and primary dendritic spacing, $\lambda_1 \propto V^{-a}G^{-b}$ (a and b represent the constants related with the alloy system), the primary spacing will increase with the increase of temperature gradient. However, when the cooling rate reaches steady state, the primary dendritic spacing will achieve stabilization gradually.

The multiple traces cladding is another important way to forming solid part, it can be carried out by overlapping cladding. Similarly, the average temperature and temperature profile of the molten pool in the overlapping direction would represent a similar thermal characteristic with multiple layer cladding of Rene88DT alloy (as shown in Fig. 14).

STRATASYS, INC. EXHIBIT 2016
IPR2025-00257, Page 6

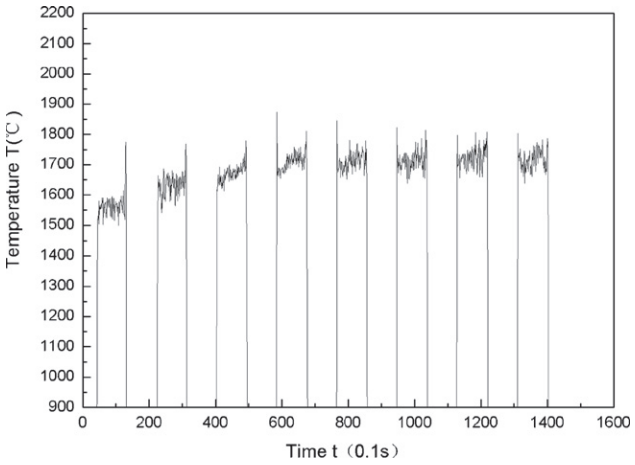


Fig. 14 – Real-time temperature measurement of the melt pool in overlap cladding.

4.3. *Relationship between molten pool temperature and layer thickness*

When the cladding process is in steady state, the energy absorbed just was used to heat the fresh powder particles being injected into the molten pool. So the following assumptions can be made before the discussion:

(1) There is no attenuation and dispersion of laser energy caused by powder particles since energy absorbed by particles will still come back to the molten pool, and the size of particle is quite small;
(2) The heat loss by convection and radiation will be neglected which is small compared to the energy input;
(3) The laser beam is of steady power, and the absorptivity for the laser and thermal properties of the materials are constant
(4) Latent heat effects are neglected because latent heat of fusion in the front is compensated by latent heat of solidification at the end of molten pool for the relatively small molten pool;
(5) The molten pool width is equal to diameter of the laser spot D_b.

Hence, on the basis of energy balance on the molten pool, the following equation can be given as

$$\beta P = Q + \eta m_p c_p \rho_p (T - T_0) \tag{2}$$

where P is the laser power, Q is the thermal conduction from molten pool, c_p is the heat capacity of the powder material, ρ_p shows the density of powder material, T_0 expresses the ambient temperature, β, m_p and η represent the absorptivity of laser energy, the powder feeding rate and the melting efficiency of powders, respectively. The second term in Eq. (2) represents the internal energy increment with the increase of temperature from initial temperature T_0 to T.

Based on the assumption of a point heat source across the substrate and constant thermal properties of materials, the heat conduction equation with a moving point heat source can be expressed as

$$\frac{\partial^2 T}{\partial x^2} + \frac{\partial^2 T}{\partial y^2} + \frac{\partial^2 T}{\partial z^2} + \frac{v_b \partial T}{\alpha \partial x} = \frac{\partial T}{\alpha \partial t} \tag{3}$$

where α is the thermal diffusivity. Further, the steady-state temperature field of a moving point heat source can be obtained as

$$T(r) = \frac{Q}{2\pi\lambda r} \exp\left(-\frac{v_b x}{2\alpha} - \frac{r v_b}{2\alpha}\right) + T_0 \tag{4}$$

where λ, r and x show the coefficient of heat conductivity, the distance from the center of heat source and the distance from the center along scanning direction, respectively. However, the new cladding layer can be considered as the heat source of the substrate. Therefore, it is assumed the molten pool as the point heat source acted on the substrate, Eq. (4) can be expressed as

$$T(r) = \frac{\beta P - \eta m_p c_p \rho_p (T' - T_0)}{2\pi\lambda r} \exp\left(-\frac{v_b x}{2\alpha} - \frac{r v_b}{2\alpha}\right) + T_0 \tag{5}$$

According to the results of fixed-point measurement on the temperature of middle point and the position of the laser beam, we can obtain the distance r_0^* correspond to the melting point temperature T_m at the boundary of molten pool and the mean temperature of molten pool T', so substituted $T(r) = T_1(r_0^*) = T_m$ and T' in Eq. (5) to yield the following equation

$$\eta m_p = \frac{\beta P - 2\pi\lambda r_0^* (T_m - T_0)}{c_p \rho_p (T' - T_0)} \tag{6}$$

According to the mass balance condition, the thickness of the cladding layer h can be calculated as follows:

$$h = \frac{\eta m_p}{D_b \rho_p v_b} \tag{7}$$

So the thickness of cladding layer can be obtained from the Eqs. (6) and (7).

Therefore, the layer thickness could be detected indirectly by measuring the molten pool temperature, and then be controlled accurately by in situ adjusting the processing parameters such as laser power, laser scanning velocity and powder feed rate.

With the constant laser power and scanning velocity, we consider r_0^* is constant and the real-time tracking measurement temperature is regarded as the mean temperature of molten pool, the control of layer thickness can be realized by using the correspondence between molten pool temperature and thickness of cladding layer. Fig. 15 shows the temperature measurement result of a single layer cladding varying with the powder feeding rate for Ni20 alloy. The powder feeding rate m_p is 5.5, 8.8 and 13.2 g/min in area I, II and III, respectively. It can be clearly found that the cladding temperature drop obviously with the increase of powder feeding rate. However, referring to the Eqs. (6) and (7), the temperature decrease will correspond to the increment of the thickness, so the layer thickness could be controlled accurately by adjusting the powder feeding rate according to the molten pool temperature.

STRATASYS, INC. EXHIBIT 2016
IPR2025-00257, Page 7

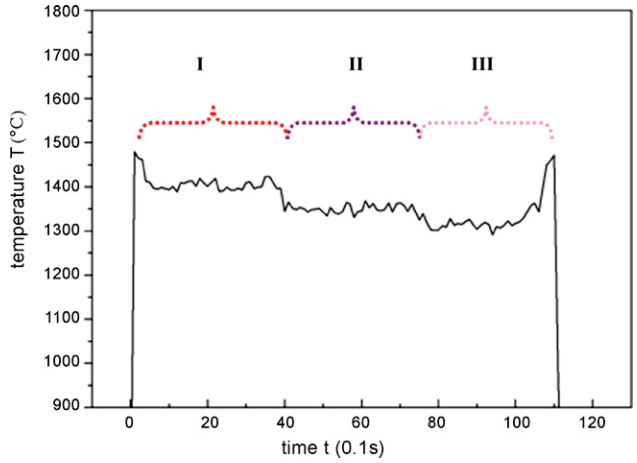


Fig. 15 – Real-time temperature measurement of the melt pool with adjusted powder feed rate.

However, in fact, the effects of size and shape of the fabricated parts during the LRF process could not be neglected, because they would affected the thermal conduction from the molten pool fatefully, especially at the edge of the part. Moreover, the cladding conditions would be changed gradually with the progress of fabrication. The appropriate adjustment should be performed according to measured temperature in order to realize parts with desired properties.

For a typical example of multiple layers or traces cladding, although all process parameters were not changed, the temperature rose gradually with the continuous cladding as shown in Figs. 12(a) and 14, however this did not mean the decrease of melting particle amounts. The rise can be considered to be caused by the accumulation of energy. With the constant powder feeding rare, the rise of molten pool temperature usually accompanied with the increase of the layer thickness, and remaining relatively steady temperature of molten pool could ensure a uniform layer thickness. Adjusting the laser power or scanning velocity means changing the input energy density. So, referring to Eq. (2), the gradual change of input energy density would solve the problem of the cumulation of energy. Fig. 16 shows the uniform temperature can be achieved by in situ adjusting the laser scanning velocity during the multi-trace cladding of Rene88DT alloy. Further, a rectangular solid Rene88DT sample with smooth surfaces was well fabricated by multi-trace and multi-layer cladding with in situ adjustment of the processing parameters based on in situ temperature measurement (as showed in Fig. 17).

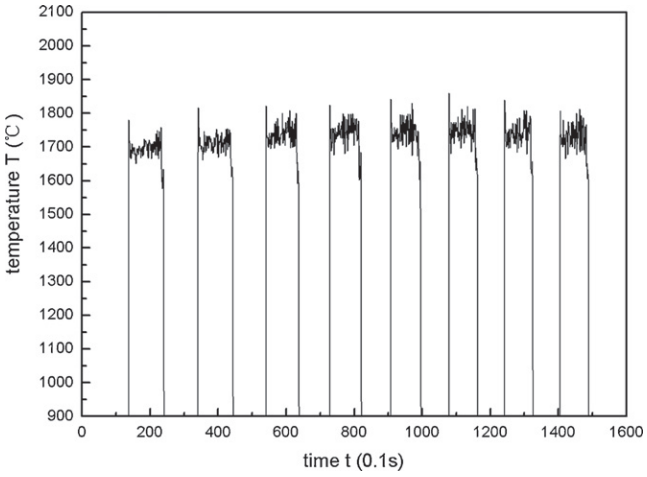


Fig. 16 – Real-time temperature measurement with adjusting the laser scanning velocity during the multiple traces cladding.

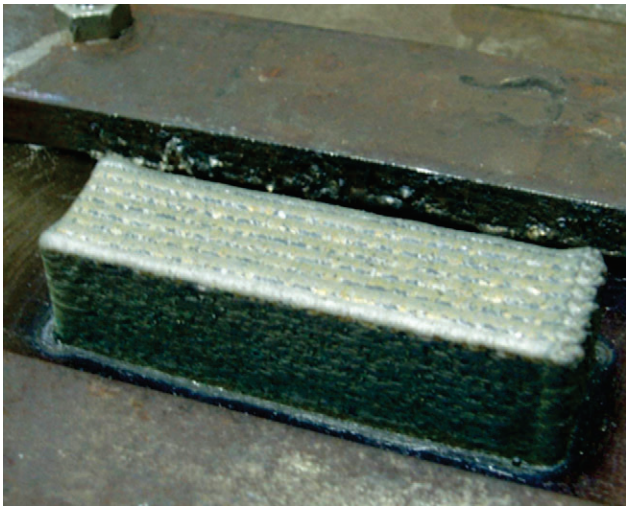


Fig. 17 – Rectangular solid sample fabricated with the adjustment of scanning velocity.

5. Conclusion

The measurement of the molten pool temperature was achieved by real-time tracking and fixed-point measurement. Based on the assumption that the molten pool is under the steady state, the temperature profile along the scanning direction was obtained from the fixed-point temperature measurement. Further, the influences of processing parameters on thermal behavior of the molten pool were acquired by some clad experiments.

The relationship between the molten pool and the thickness of cladding layer was also discussed, which give a possible scheme to achieve in situ accurate control for the layer thickness by using an analytical model based on temperature measurement of the molten pool. When laser power and scanning velocity are constant, the cladding thickness only corresponds to molten pool temperature, so the layer thickness may be controlled accurately by in situ adjusting powder feeding rate according to molten pool temperature.

A smooth solid sample was fabricated successfully by in situ adjusting the processing parameters with the feedback of molten pool temperature.

Acknowledgements

The authors would like to express their gratitude to National Natural Science Foundation of China (Grant No. 50331010)

STRATASYS, INC. EXHIBIT 2016
IPR2025-00257, Page 8

and Talent Cultivating Program of Northwestern Polytechnical University (Grant No. 05XE0131). The work was also supported by Program for New Century Excellent Talents in University of China.

REFERENCES

Griffith, M.L., Schlienger, M.E., Harwell, L.D., et al., 1999. Understanding thermal behavior in the LENS process. Mater. Design 20, 107–113.

Han, L., Liou, F.W., Phatak, K.M., 2004. Modeling of laser cladding with powder injection. Metall. Mater. Trans. B 35 (6), 1139–1150.

Hand, D.P., Fox, M.D.T., 2000. Optical focus control system for laser welding and direct casting. Opt. Lasers Eng. 34, 415–427.

Hu, D., Kovacevic, R., 2003. Sensing, modeling and control for laser-based additive manufacturing. Int. J. Machine Tools Manuf. 43, 51–60.

Hu, D., Mei, H., Kovacevic, R., 2002. Improving solid freeform fabrication by laser based additive manufacturing. Proceedings of the Institution of Mechanical Engineers. Part B: J. Eng. Manuf. 216 (9), 1253–1264.

Jendrzejewski, R., Kreja, I., Śliwiński, G., 2004. Temperature distribution in laser-clad multi-layers. Mater. Sci. Eng. A 379, 313–320.

Keicher, D.M., Smugeresky, J.E., Romero, J.A., Griffith, M.L., Harwell, L.D., 1997. SPIE 2293, 91–97.

Lin, J., Steen, W.M., 1998. An in-process method for the inverse estimaton of the powder catchment efficiency during laser cladding. Opt. Technol. 30, 77–84.

Wu, X., Mei, J., 2003. Near net shape manufacturing of components using direct laser fabrication technology. J. Mater. Process. Technol. 135, 266–270.

STRATASYS, INC. EXHIBIT 2016
IPR2025-00257, Page 9